



# Partial Invariants, Large-scale Dynamo Action, and the Inverse Transfer of Magnetic Helicity

Nicholas M. Rathmann and Peter D. Ditlevsen

Niels Bohr Institute, University of Copenhagen, Denmark; [rathmann@nbi.ku.dk](mailto:rathmann@nbi.ku.dk)*Received 2019 March 26; revised 2019 October 18; accepted 2019 October 29; published 2019 December 13*

## Abstract

The existence of partially conserved enstrophy-like quantities is conjectured to cause inverse energy transfers to develop embedded in magnetohydrodynamical (MHD) turbulence, in analogy to the influence of enstrophy in two-dimensional nonconducting turbulence. By decomposing the velocity and magnetic fields in spectral space onto helical modes, we identify subsets of three-wave (triad) interactions conserving two new enstrophy-like quantities that can be mapped to triad interactions recently identified with facilitating large-scale  $\alpha$ -type dynamo action and the inverse transfer of magnetic helicity. Due to their dependence on interaction scale locality, invariants suggest that the inverse transfer of magnetic helicity might be facilitated by both local- and nonlocal-scale interactions, and is a process more local than the  $\alpha$ -dynamo. We test the predicted embedded (partial) energy fluxes by constructing a shell model (reduced wave-space model) of the minimal set of triad interactions (MTI) required to conserve the ideal MHD invariants. Numerically simulated MTIs demonstrate that, for a range of forcing configurations, the partial invariants are, with some exceptions, indeed useful for understanding the embedded contributions to the total spectral energy flux. Furthermore, we demonstrate that strictly inverse energy transfers may develop if enstrophy-like conserving interactions are favored, a mechanism recently attributed to the energy cascade reversals found in nonconducting three-dimensional turbulence subject to strong rotation or confinement. The presented results have implications for the understanding of the physical mechanisms behind large-scale dynamo action and the inverse transfer of magnetic helicity, processes thought to be central to large-scale magnetic structure formation.

*Key words:* dynamo – magnetic fields – magnetohydrodynamics (MHD) – turbulence

## 1. Introduction

A central problem in astrophysics is understanding how large-scale magnetic fields are generated by astrophysical bodies such as planets, stars, and galaxies (Parker 1979). A popular explanation is that large-scale dynamo action occurs, which allows a small magnetic seed field to grow by stretching, twisting, and folding through interactions with the velocity field inside the electroconducting fluid of the body, whereby kinetic energy is converted to magnetic energy (Moffatt 1978; Krause & Rädler 1980; Brandenburg & Subramanian 2005; Tobias et al. 2013). A celebrated example of a large-scale dynamo is the  $\alpha$ -effect of mean-field electrodynamics (Steenbeck et al. 1966; Moffatt 1978; Krause & Rädler 1980), where the mean electromotive force caused by small-scale field fluctuations is related to the large-scale magnetic field by a coefficient,  $\alpha$ . In the presence of small-scale kinetic helicity (net imbalance between left- and right-handed helical motion), the  $\alpha$ -effect leads to the development of large- and small-scale magnetic helicity of opposite signs, where the small-scale magnetic and kinetic helicity share signs (Brandenburg & Subramanian 2005). This process can conceptually be related to a stretch–twist–fold dynamo for closed magnetic flux tubes which generates opposite signs of magnetic helicity at large and small scales (Vainshtein & Zel'Dovich 1972; Childress & Gilbert 1995). Combining the  $\alpha$ -effect with the influence of differential rotation ( $\omega$ -effect), the  $\alpha$ - $\omega$  dynamo (Moffatt 1978; Parker 1979; Krause & Rädler 1980) has widely been invoked to explain the amplification and maintenance of large-scale magnetic fields. In spiral galaxies, for example, this mechanism leads to predicted magnetic (spiral) pitch angles in the middle of observed ranges (Widrow 2002; Brandenburg & Subramanian 2005), among

other observations in support of dynamo action (Shukurov 2004). Likewise, large-scale solar magnetic phenomena, such as solar flares and spots, are generally attributed to dynamo action in combination with differential rotation within the solar convective zone (Hood & Hughes 2011; Brun & Browning 2017).

Magnetic helicity is an inviscid integral of motion in magnetohydrodynamical (MHD) turbulence, and is observed in, e.g., the solar photosphere (Démoulin 2007; Blackman 2016) and the solar wind (Howes & Quataert 2010), and plays a role in coronal mass ejections by effecting magnetic flux tube topologies (Malapaka & Müller 2013a). The inverse (upscale) transfer of magnetic helicity (Frisch et al. 1975) is another transfer process suggested to contribute to large-scale magnetic structure formation by virtue of the spectral bounds between magnetic energy and magnetic helicity (Pouquet et al. 1976; Moffatt 1978; Biskamp 1993). In spite of receiving a lot of attention, less is known about the nonlinear dynamics enabling an inverse transfer of magnetic helicity.

Simulations of homogeneous MHD turbulence in a box with triple periodic boundaries have been the subject of many studies attempting to better understand the conditions under which large-scale magnetic structure formation takes place due to the  $\alpha$ -effect (Brandenburg 2001; Linkmann et al. 2017) and the inverse transfer of magnetic helicity (Alexakis et al. 2006; Müller et al. 2012; Malapaka & Müller 2013b; Linkmann & Dallas 2016, 2017; Linkmann et al. 2017). As an outcome, different degrees of scale locality among interactions between fields have been reported, and it is currently thought that long-range interactions might be more important in MHD turbulence than in nonconducting fluids (Mininni 2011). On this note, we

shall refrain from referring to the inverse transfer of magnetic helicity as a cascade process, since the latter is generally associated with a constant flux through wavenumber space due to scale-local interactions, which the transfer of magnetic helicity might not be (Alexakis et al. 2006; Aluie & Eyink 2010; Müller et al. 2012).

In an attempt to better understand the mechanisms that facilitate large-scale magnetic structure formation of astrophysical interest, such as the inverse transfer of magnetic helicity and large-scale dynamo action, it is therefore important to study the nonlinear dynamics by which inviscid invariants are transferred across spatial scales. This is the focus of our work.

### 1.1. Role of Inviscid Invariants

In three-dimensional (3D), isotropic, hydrodynamical (HD) turbulence, kinetic energy is, on average, transferred from the large integral (pumping) scale of motion to the small, dissipative Kolmogorov scale (where it is dissipated as heat) by scale-local interactions, called a forward or direct energy cascade. In certain cases of HD turbulence, however, such as two-dimensional (2D) flows (Boffetta & Musacchio 2010; Mininni & Pouquet 2013) and strongly rotating 3D flows with a broken mirror symmetry (Sulem et al. 1989; Mininni et al. 2009), an inverse (or reverse) energy cascade has been observed.

In 3D HD turbulence, the dissipation of energy at the Kolmogorov scale is proportional to the enstrophy (vorticity squared) at this scale. The energy cascade in high Reynolds number turbulence must therefore be facilitated by a production of enstrophy, which is possible by means of the stretching and bending term in the vorticity equation. In 2D HD turbulence, however, the stretching and bending term is absent, and enstrophy, too, is an inviscid invariant along with energy and can only grow by increased pumping. Because the energy spectrum,  $E(k)$ , and the enstrophy spectrum,  $Z(k)$ , are related by  $Z(k) = k^2 E(k)$ , the cascades of the two quantities cannot be treated independently, which leads to dual and counter-directional cascades whereby enstrophy cascades forwardly and energy cascades inversely (Kraichnan 1967; Alexakis & Biferale 2018).

In 3D HD flows, a second inviscid invariant also exists: kinetic helicity, defined as the integral of the inner product between velocity and vorticity (Moffatt 1969; Brissaud et al. 1973; Kraichnan 1973). In contrast to enstrophy in 2D, the effect of helicity on the directionality of the energy cascade in 3D is less well understood. Although the helicity spectrum can also dominate over the energy spectrum at small scales (large wavenumber,  $k$ ) as enstrophy, helicity is not sign definite as opposed to enstrophy. As a consequence, helicity does not place similar restrictions on the direction of the energy cascade (Alexakis & Biferale 2018).

By decomposing the velocity field in spectral space onto helical modes, each velocity component evolves according to the Navier–Stokes equation by helical three-wave (triad) interactions which separately conserve kinetic energy and kinetic helicity (Constantin & Majda 1988; Waleffe 1992). Recently, new additional quantities were identified that are partially conserved among helical triad interactions (De Pietro et al. 2015; Rathmann & Ditlevsen 2016, 2017), henceforth referred to as pseudo-invariants or partial invariants; that is, quantities which are conserved only by a subset of all possible helical triad interactions. In a further subset of helical triad interactions, the associated pseudo-invariants become

enstrophy-like and have been suggested to induce embedded (partial) inverse energy cascades in 3D HD turbulence (Rathmann & Ditlevsen 2017) (relevant to the interpretation of other numerical studies, e.g., Biferale et al. 2012; De Pietro et al. 2015; Alexakis 2017; Sahoo et al. 2017a). Since these triad interactions are predominantly responsible for channeling energy upscale within rotating flows (Buzzicotti et al. 2018), and with possible relevance for thin-layered turbulence (Benavides & Alexakis 2017), there are reasons to believe that inverse energy transfers might generally exist embedded in 3D HD turbulence due to partial invariants with implications for the net transfer of energy.

In ideal MHD turbulence, the existence of three inviscid invariants involving the velocity and magnetic fields, and the existence of separate dissipation scales associated with kinematic viscosity and magnetic resistivity, make understanding the factors controlling transfer processes particularly challenging. For example, in the nonlinear regime where the back-reaction on the velocity field from the Lorentz force is non-negligible, the inverse transfer of magnetic helicity may be more or less local in scale depending on the relative signs of the small-scale kinetic helicity and magnetic helicity content (Linkmann et al. 2017). Inverse spectral transfers can, however, occur even for vanishing kinetic and magnetic helicity (Brandenburg et al. 2015), and Aluie (2017) showed that the transfer directionality of magnetic helicity depends on the magnetic Reynolds number (high values excluding a forward transfer). Meanwhile, Bian & Aluie (2019) recently demonstrated the existence of a subrange within the inertial-inductive range in which the total energy cascade decouples into separate, conservative cascades of kinetic and magnetic energy.

Because of their clear physical interpretation, quadratic invariants, such as enstrophy, play a central role in the study of turbulent cascade dynamics. In this work, we conjecture that the spectral–helically decomposed energy fluxes in ideal MHD turbulence might also be understood in terms of pseudo-invariants, which has potential implications for large-scale magnetic structure formation insofar as the aggregate of triads interactions conserving them are relevant for the velocity and magnetic field evolutions. We show that two new enstrophy-like quantities are partially conserved by the ideal MHD equations, and argue that embedded, inverse energy transfers might develop as a result. Intriguingly, the new quantities are conserved by triad interactions recently argued to facilitate large-scale  $\alpha$ -type dynamo action and the inverse transfer of magnetic helicity (Linkmann et al. 2016). By constructing a shell model (reduced wave-space model), we show the new pseudo-invariants are indeed useful for understanding the simulated partial (forward and inverse) spectral energy fluxes and, moreover, demonstrate that strictly inverse energy transfers might develop if enstrophy-like conserving interactions are favored, such as results for nonconducting turbulence subject to strong rotation (Buzzicotti et al. 2018) or confinement (Benavides & Alexakis 2017) suggest.

## 2. The Spectral–Helical Decomposition

In real space, the incompressible, ideal MHD equations are

$$\begin{aligned} (\partial_t - \nu \nabla^2) \mathbf{u} &= -(\mathbf{u} \cdot \nabla) \mathbf{u} + (\nabla \mathbf{B}) \times \mathbf{B} - \nabla p \\ (\partial_t - \eta \nabla^2) \mathbf{B} &= (\mathbf{B} \cdot \nabla) \mathbf{u} - (\mathbf{u} \cdot \nabla) \mathbf{B} \\ \nabla \cdot \mathbf{u} &= 0 \quad \text{and} \quad \nabla \cdot \mathbf{B} = 0, \end{aligned} \tag{1}$$

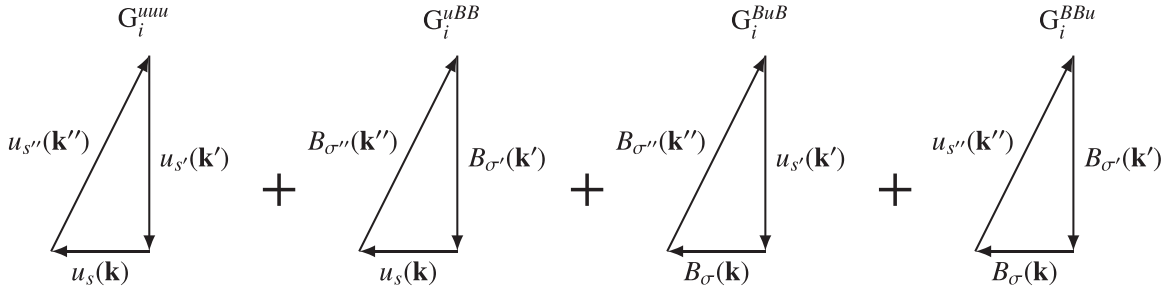


**Figure 1.** Minimal set of helical triad interactions (MTI) required to conserve all three magnetohydrodynamical invariants. For a given triad of waves,  $\{\mathbf{k}, \mathbf{k}', \mathbf{k}''\}$ , the MTI consists of four components per possible combination of helical signs of the interacting modes  $\{s, s', s'', \sigma, \sigma', \sigma''\}$  (or sign group numbers  $i$ ; see the text): one velocity triad interaction ( $G_i^{uuu}$ ) and three velocity–magnetic triad interactions ( $G_i^{uBB}$ ,  $G_i^{BuB}$ ,  $G_i^{BBu}$ ). The behavior of the MTI components is proposed to be explained by the conservation (or lack thereof) of a pseudo-invariant quantity,  $E^{(\omega)}$ .

where  $\mathbf{u}$  is the velocity field,  $\mathbf{B}$  the magnetic field in Alfvén units,  $\nu$  is the kinematic viscosity,  $\eta$  the magnetic resistivity,  $p$  the pressure, and the density is set to  $\rho = 1$  for convenience. In spectral space, the divergence-free constraints on  $\mathbf{u}$  and  $\mathbf{B}$  translate into  $\mathbf{k} \cdot \mathbf{u}(\mathbf{k}) = 0$  and  $\mathbf{k} \cdot \mathbf{B}(\mathbf{k}) = 0$ . The helical basis (Constantin & Majda 1988; Waleffe 1992) exploits this property by decomposing each complex spectral component into two helical modes,  $\mathbf{h}_{\pm}(\mathbf{k})$ , which are mutually perpendicular to  $\mathbf{k}$  and are eigenmodes of the curl operator, i.e.,  $i\mathbf{k} \times \mathbf{h}_{\pm} = \pm k\mathbf{h}_{\pm}$  where  $k = |\mathbf{k}|$ . In this basis, the velocity and magnetic components are given by

$$\begin{aligned} \mathbf{u}(\mathbf{k}) &= u_+(\mathbf{k})\mathbf{h}_+ + u_-(\mathbf{k})\mathbf{h}_- \\ \mathbf{B}(\mathbf{k}) &= B_+(\mathbf{k})\mathbf{h}_+ + B_-(\mathbf{k})\mathbf{h}_-, \end{aligned}$$

and the ideal MHD invariants energy ( $E$ ), magnetic helicity ( $H_m$ ), and cross-helicity ( $H_c$ ), are given by

$$E = \sum_{\mathbf{k}} E(\mathbf{k}) = \sum_{\mathbf{k}} \sum_s \frac{1}{2} (|u_s(\mathbf{k})|^2 + |B_s(\mathbf{k})|^2) \quad (2)$$

$$H_m = \sum_{\mathbf{k}} H_m(\mathbf{k}) = \sum_{\mathbf{k}} \sum_s \frac{s}{k} |B_s(\mathbf{k})|^2 \quad (3)$$

$$H_c = \sum_{\mathbf{k}} H_c(\mathbf{k}) = \sum_{\mathbf{k}} \sum_s \text{Re} [u_s(\mathbf{k})B_s^*(\mathbf{k})], \quad (4)$$

where  $s = \pm 1$  is a helical sign coefficient, and  $E(\mathbf{k})$ ,  $H_m(\mathbf{k})$ , and  $H_c(\mathbf{k})$  are the respective spectra.

Lessinnes et al. (2009) first proposed applying the decomposition also to the MHD Equations (1), giving

$$\begin{aligned} &(\partial_t + \nu k^2)u_s(\mathbf{k}) \\ &= \sum_{\mathbf{k}+\mathbf{k}'+\mathbf{k}''=0} \left( \sum_{s',s''} (s'k' - s''k'') g_{ss's''} u_{s'}^*(\mathbf{k}') u_{s''}^*(\mathbf{k}'') \right. \\ &\quad \left. - \sum_{\sigma',\sigma''} (\sigma'k' - \sigma''k'') g_{\sigma\sigma'\sigma''} B_{\sigma'}^*(\mathbf{k}') B_{\sigma''}^*(\mathbf{k}'') \right) \quad (5) \end{aligned}$$

$$\begin{aligned} &(\partial_t + \eta k^2)B_{\sigma}(\mathbf{k}) = \sigma k \sum_{\mathbf{k}+\mathbf{k}'+\mathbf{k}''=0} \\ &\quad \times \left( \sum_{\sigma',\sigma''} g_{\sigma\sigma'\sigma''} B_{\sigma'}^*(\mathbf{k}') u_{\sigma''}^*(\mathbf{k}'') - \sum_{s',s''} g_{\sigma s' s''} u_{s'}^*(\mathbf{k}') B_{\sigma''}^*(\mathbf{k}'') \right), \quad (6) \end{aligned}$$

where  $\{s, s', s'', \sigma, \sigma', \sigma''\} = \pm 1$  are helical sign coefficients of the interacting helical modes, and

$$g_{ss's''} = -1/4 \mathbf{h}_s^*(\mathbf{k}') \times \mathbf{h}_{s''}^*(\mathbf{k}'') \cdot \mathbf{h}_s^*(\mathbf{k})$$

is an interaction coefficient. Velocity modes  $u_s(\mathbf{k})$  thus evolve by helical triad (three-wave) interactions involving  $\{u_{s'}(\mathbf{k}'), u_{s''}(\mathbf{k}'')\}$  and  $\{B_{\sigma'}(\mathbf{k}'), B_{\sigma''}(\mathbf{k}'')\}$ , while magnetic modes  $B_{\sigma}(\mathbf{k})$  evolve by helical triad interactions involving  $\{u_{s'}(\mathbf{k}'), B_{\sigma''}(\mathbf{k}'')\}$  and  $\{B_{\sigma'}(\mathbf{k}'), u_{s''}(\mathbf{k}'')\}$ , provided that triads close ( $\mathbf{k} + \mathbf{k}' + \mathbf{k}'' = 0$ ).

Note that the splitting of the curl of the electromotive force  $\nabla \times (\mathbf{u} \times \mathbf{B})$  in the induction equation into an advective term,  $(\mathbf{u} \cdot \nabla)\mathbf{B}$ , and dynamo (stretching) term,  $(\mathbf{B} \cdot \nabla)\mathbf{u}$ , is obfuscated by the spectral–helical decomposition and these terms are therefore not directly associated with the two sums in (6).

For each of the four types of helical triad interactions,  $2^3 = 8$  distinct combinations of helical signs are possible as indicated by the sums over the helical signs in (5), (6). If sorted against shared interaction coefficients, however, only four unique sign combinations remain per triad type: for each of the triad types  $\{u_s(\mathbf{k}), u_{s'}(\mathbf{k}'), u_{s''}(\mathbf{k}'')\}$ ,  $\{u_s(\mathbf{k}), B_{\sigma'}(\mathbf{k}'), B_{\sigma''}(\mathbf{k}'')\}$ ,  $\{B_{\sigma}(\mathbf{k}), u_{s'}(\mathbf{k}'), B_{\sigma''}(\mathbf{k}'')\}$ , and  $\{B_{\sigma}(\mathbf{k}), B_{\sigma'}(\mathbf{k}'), u_{s''}(\mathbf{k}'')\}$ , the associated helical signs  $\{s, s', s''\}$ ,  $\{s, \sigma', \sigma''\}$ ,  $\{\sigma, s', \sigma''\}$ , and  $\{\sigma, \sigma', s''\}$ , respectively, may be any one of the combinations  $\pm\{+, -, +\}$ ,  $\pm\{+, -, -\}$ ,  $\pm\{+, +, -\}$ , and  $\pm\{+, +, +\}$ . From here on, these four possible combinations of helical signs shall be referred to as sign groups  $i = 1, 2, 3, 4$ , respectively. Any particular helical triad interaction may therefore be referred to by a combination of the triad type and its sign group number, henceforth denoted compactly by  $G_i^{XYZ}$ . In this notation,  $i$  refers to the sign group number, and  $X, Y$ , and  $Z$  are placeholders for the fields of the interacting modes. Note that only the four types  $XYZ \in \{uuu, uBB, BuB, BBu\}$  exist, and that  $X$  is the field associated with wave-vector  $\mathbf{k}$ ,  $Y$  with  $\mathbf{k}'$ , and  $Z$  with  $\mathbf{k}''$ .

Isolating terms in (5), (6) involving a single triad of waves,  $\{\mathbf{k}, \mathbf{k}', \mathbf{k}''\}$ , only four triad interactions remain per possible combination of helical signs, namely  $G_i^{uuu} + G_i^{uBB} + G_i^{BuB} + G_i^{BBu}$ , hereafter referred to as a minimal set of triad interactions (MTI) following Linkmann et al. (2017) (Figure 1). Note that  $2^6 = 64$  distinct MTIs are possible, and that only in the case of homochiral MTIs ( $s = \sigma, s' = \sigma',$  and  $s'' = \sigma''$ ) do the four MTI components share sign group numbers ( $i$ ).

By noting the cyclic property of  $g_{ss's''}$ , the evolution of velocity and magnetic modes in a given MTI is governed

by (Linkmann et al. 2016)

$$\begin{aligned}
d_t u_s &= (s'k' - s''k'')g_{ss's''}u_s^*u_{s'}^*u_{s''}^* \\
&\quad - (\sigma'k' - \sigma''k'')g_{\sigma\sigma'\sigma''}B_\sigma^*B_{\sigma'}^*B_{\sigma''}^* \\
d_t u_{s'} &= (s''k'' - sk)g_{ss's''}u_s^*u_{s'}^*u_{s''}^* \\
&\quad - (\sigma''k'' - \sigma k)g_{\sigma\sigma'\sigma''}B_\sigma^*B_{\sigma'}^*B_{\sigma''}^* \\
d_t u_{s''} &= (sk - s'k')g_{ss's''}u_s^*u_{s'}^*u_{s''}^* \\
&\quad - (\sigma k - \sigma'k')g_{\sigma\sigma'\sigma''}B_\sigma^*B_{\sigma'}^*B_{\sigma''}^* \\
d_t B_\sigma &= \sigma k (g_{\sigma\sigma'\sigma''}B_\sigma^*u_{s'}^*u_{s''}^* - g_{\sigma\sigma'\sigma''}u_s^*B_{\sigma'}^*B_{\sigma''}^*) \\
d_t B_{\sigma'} &= \sigma'k' (g_{\sigma\sigma'\sigma''}B_\sigma^*u_s^*u_{s''}^* - g_{\sigma\sigma'\sigma''}u_{s'}^*B_\sigma^*B_{\sigma''}^*) \\
d_t B_{\sigma''} &= \sigma''k'' (g_{\sigma\sigma'\sigma''}B_\sigma^*u_s^*u_{s'}^* - g_{\sigma\sigma'\sigma''}u_{s''}^*B_\sigma^*B_{\sigma'}^*), \quad (7)
\end{aligned}$$

where the compact notations  $u_s = u_s(\mathbf{k})$ ,  $u_{s'} = u_{s'}(\mathbf{k}')$ , and  $u_{s''} = u_{s''}(\mathbf{k}'')$  are used (and likewise for  $B$ ). While the relative magnitudes of energy, magnetic helicity, and cross-helicity fluxes between the three triad legs are fixed and determined by the coefficients in (7), the magnitudes and directions of the average fluxes (to or from a leg) depend on the unknown triple-correlators  $\langle u_s^*u_{s'}^*u_{s''}^* \rangle + \text{c.c.}$ ,  $\langle u_s^*B_{\sigma'}^*B_{\sigma''}^* \rangle + \text{c.c.}$ ,  $\langle B_\sigma^*u_{s'}^*B_{\sigma''}^* \rangle + \text{c.c.}$ , and  $\langle B_\sigma^*B_{\sigma'}^*u_{s''}^* \rangle + \text{c.c.}$ .

From this simpler form of the spectral dynamics, it follows that each MTI conserves energy, magnetic helicity, and cross-helicity, by noting

$$\begin{aligned}
d_t [E(\mathbf{k}) + E(\mathbf{k}') + E(\mathbf{k}'')] &= 0 \\
d_t [H_m(\mathbf{k}) + H_m(\mathbf{k}') + H_m(\mathbf{k}'')] &= 0 \\
d_t [H_c(\mathbf{k}) + H_c(\mathbf{k}') + H_c(\mathbf{k}'')] &= 0.
\end{aligned}$$

The ideal MHD invariants (2)–(4) are thus conserved per triad of waves, but only collectively by the four components  $G_i^{uuu} + G_i^{uBB} + G_i^{BuB} + G_i^{BBu}$  constituting an MTI (for any choice of helical signs), hence the notion of a minimal set.

Linkmann et al. (2016) recently proposed the behavior of a given MTI might be understood from the linear stability of (7) around trivial steady states, inspired by a similar approach in HD turbulence (Waleffe 1992). Waleffe suggested that energy, on average, flows from the most unstable triad mode (leg) and into the other two. In this regard, the behavior of a given triad may be classified as either forward (F-class) if the smallest wavenumber mode (largest scale) is linearly unstable, suggesting that energy is transferred to the two smaller scales (forward cascade), or reverse (R-class) if either the middle or largest wavenumber modes are unstable, suggesting that energy is transferred either partly or fully to larger scales (inverse cascade). By considering the linear stability of the states  $\{u_s^*, u_{s'}^*, u_{s''}^*, B_\sigma^*, B_{\sigma'}^*, B_{\sigma''}^*\} = \{u_0, 0, 0, B_0, 0, 0\}$ ,  $\{0, u_0, 0, 0, B_0, 0\}$ ,  $\{0, 0, U_0, 0, 0, B_0\}$ , where  $u_0$  and  $B_0$  are constants, Linkmann et al. (2016) showed that the modes  $x_i = (u_s, B_\sigma)$  evolve by  $\dot{x}_i = M_{ij}x_j$  (and similarly for  $x_i = (u_{s'}, B_{\sigma'})$ ,  $(u_{s''}, B_{\sigma''})$ , but with different  $M_{ij}$ ). The modal (leg) stabilities therefore depend on the existence eigenvalues for  $M_{ij}$  with real, positive parts, which have complicated dependences compared to the HD case: in addition to  $M_{ij}$  depending on the helical signs of the three interacting modes, such as a stability analysis of the pure HD case also does, it moreover depends on the ratio  $u_0/B_0$ , and the alignment between velocity and magnetic modes (cross-helicity).

In fully developed turbulence, it is, however, not immediately clear to what extent the stability properties of isolated

triads are applicable to the full network of triad interactions as represented by the Navier–Stokes equation (Moffatt 2014). Several numerical HD studies considering both decimated (biased) and unbiased triad networks, as well as studies on thin-layer turbulence and flows subject to strong rotation, suggest meanwhile that the stability properties are indeed useful for explaining the embedded (partial) flux contributions to the total energy flux, including forward–inverse transitions of the total energy flux (see the review by Alexakis & Biferale 2018). Extending to the MHD case, Linkmann et al. (2017) recently considered which triad interactions might be associated with large- and small-scale dynamo action and the inverse transfer of magnetic helicity, finding numerically that the helical signature of the resulting large- and small-scale magnetic field components is consistent with the influence of dominant triad interactions according to a linear stability analysis, thus demonstrating its usefulness also in MHD turbulence.

Despite the predictive skill of triad stability analyses, attributing the predicted behaviors to physical mechanisms is still an open problem, one which this work attempts to address in terms of partially conserved quantities among triad interactions (pseudo-invariants).

### 3. Pseudo-invariants

In HD turbulence, quadratic invariants play a fundamental role in the understanding of turbulent cascade dynamics, such as the energy cascade reversal in 2D which may be understood by both energy and enstrophy being strictly positive quantities and enstrophy dominating the small scales (Alexakis & Biferale 2018). The fact that  $G_4^{uuu}$  interactions in 3D conserve both signs of kinetic helicity separately is an intriguing possible explanation for the identified R-class nature of  $G_4^{uuu}$  interactions (Biferale et al. 2012) in analogy to enstrophy-conserving interactions in 2D. Recently, the mixed forward–inverse behavior exhibited by  $G_2^{uuu}$  interactions depending on triad geometry (Waleffe 1992; De Pietro et al. 2015; Rathmann & Ditlevsen 2017) was also proposed to be explained by the existence of a new enstrophy-like pseudo-invariant  $E^{(\alpha)}(\mathbf{k}) = k^\alpha (|u_+(\mathbf{k})|^2 + |u_-(\mathbf{k})|^2)$ , where  $\alpha \in \mathbb{R}$  depends on the specific triad shape  $\{k, k', k''\}$  and hence interaction locality in wave space (Rathmann & Ditlevsen 2017).

Following Rathmann & Ditlevsen (2017), we here show that a subset of MHD triad interactions exists that also conserves enstrophy-like quantities, which might help in understanding the behavior of MTIs in terms of conserved quantities in analogy to enstrophy-conserving interactions in 2D HD turbulence. Inspired by the HD pseudo-invariant, consider therefore the generalized spectral energy density defined as

$$E^{(\alpha)}(\mathbf{k}) = k^\alpha (|u_+(\mathbf{k})|^2 + |u_-(\mathbf{k})|^2 + |B_+(\mathbf{k})|^2 + |B_-(\mathbf{k})|^2). \quad (8)$$

This quantity is thus enstrophy-like for exponents  $\alpha > 0$ , and might induce an inverse (upscale) contribution to the total transfer of energy if conserved by triad interactions. Note that  $\alpha = 0$  corresponds to energy which is conserved by any MTI.

Applying (7) to (8), it follows that the pseudo-invariant is conserved if  $d_t [E^{(\alpha)}(\mathbf{k}) + E^{(\alpha)}(\mathbf{k}') + E^{(\alpha)}(\mathbf{k}'')] = 0$ , implying

$$\begin{aligned}
k^{\alpha+1} [L^{uuu}(\alpha)g_{ss's''}u_s^*u_{s'}^*u_{s''}^* - L^{uBB}(\alpha)g_{\sigma\sigma'\sigma''}u_s^*B_{\sigma'}^*B_{\sigma''}^* \\
- L^{BuB}(\alpha)g_{\sigma\sigma'\sigma''}B_\sigma^*u_{s'}^*B_{\sigma''}^* + L^{BBu}(\alpha)g_{\sigma\sigma'\sigma''}B_\sigma^*B_{\sigma'}^*u_{s''}^* \\
+ \text{c.c.}] = 0,
\end{aligned}$$

where (suppressing dependences on wavenumbers and helical signs in the definitions of  $L^{XYZ}(\alpha)$ )

$$L^{uuu}(\alpha) = \left( s' \frac{k'}{k} - s'' \frac{k''}{k} \right) + \left( s'' \frac{k''}{k} - s \right) \left( \frac{k'}{k} \right)^\alpha + \left( s - s' \frac{k'}{k} \right) \left( \frac{k''}{k} \right)^\alpha \quad (9)$$

$$L^{uBB}(\alpha) = \left( \sigma' \frac{k'}{k} - \sigma'' \frac{k''}{k} \right) - \sigma' \left( \frac{k'}{k} \right)^{\alpha+1} + \sigma'' \left( \frac{k''}{k} \right)^{\alpha+1} \quad (10)$$

$$L^{BuB}(\alpha) = \sigma + \left( \sigma'' \frac{k''}{k} - \sigma \right) \left( \frac{k'}{k} \right)^\alpha - \sigma'' \left( \frac{k''}{k} \right)^{\alpha+1} \quad (11)$$

$$L^{BBu}(\alpha) = \sigma - \sigma' \left( \frac{k'}{k} \right)^{\alpha+1} + \left( \sigma' \frac{k'}{k} - \sigma \right) \left( \frac{k''}{k} \right)^\alpha. \quad (12)$$

Conservation by an MTI thus requires the existence of solutions  $\alpha \in \mathbb{R}$  that simultaneously fulfil  $L^{XYZ}(\alpha) = 0$  for all  $XYZ \in \{uuu, uBB, BuB, BBu\}$ . Since this is not possible, we are here interested in the possibility that the four individual MTI components (Figure 1) might separately conserve different pseudo-invariants, leading to inverse partial fluxes developing.

Equations (9)–(12) are functions of the wavenumber ratios  $k'/k$  and  $k''/k$ , and consist of a constant term and two monotonically increasing or decreasing terms. Thus, the pseudo-invariants depend on triad shape and hence interaction locality. For solutions  $L^{XYZ}(\alpha) = 0$  to exist besides energy ( $\alpha = 0$ ), the signs of the three terms in each of (9)–(12) must alternate (considering the ordering  $k \leq k' \leq k''$  without loss of generality). On inspection, it follows that only interactions  $G_i^{XYZ} \in \{G_2^{uuu}, G_4^{uuu}, G_2^{BuB}, G_3^{BuB}, G_3^{BBu}, G_4^{BBu}\}$  solve  $L^{XYZ}(\alpha) = 0$  for  $\alpha \neq 0$ .

The HD pseudo-invariant associated with  $G_2^{uuu}$  triads has previously been investigated (Rathmann & Ditlevsen 2017), finding a cascade reversal indeed takes place for a nonlocal subset of triad geometries due to the invariant becoming enstrophy-like ( $\alpha > 0$ ). The pseudo-invariant associated with the velocity–magnetic triads  $G_2^{BuB}$ ,  $G_3^{BuB}$ ,  $G_3^{BBu}$ , and  $G_4^{BBu}$  have, however, not previously been considered. Unlike the HD  $L$ -term (9), the  $L$ -terms (10)–(12) do not depend on the helical signs of all three triad legs: the helical sign of the velocity mode does not enter (10)–(12), implying  $G_2^{BuB}$  and  $G_3^{BuB}$  share  $L$ -terms, and thus pseudo-invariants, as do  $G_3^{BBu}$  and  $G_4^{BBu}$ .

Figures 2(a) and (b) show the numerical solutions w.r.t.  $\alpha$  for  $L^{BuB}(\alpha) = 0$  and  $L^{BBu}(\alpha) = 0$ , respectively, hereafter referred to as  $\alpha^{BuB}$  and  $\alpha^{BBu}$ . The solutions are shown for all possible (noncongruent) triad geometries (colored area) by expressing each triad in terms of the two interior angles  $\theta'$  and  $\theta''$  using the sine rule:  $k'/k = \sin(\theta'')/\sin(\pi - \theta' - \theta'')$  and  $k''/k = \sin(\theta')/\sin(\pi - \theta' - \theta'')$ . Figure 2(a) shows that  $G_2^{BuB}$  and  $G_3^{BuB}$  interactions may, similarly to  $G_2^{uuu}$ , contribute either to a forward transfer of energy ( $\alpha^{BuB} < 0$ , blue colors) or inversely ( $\alpha^{BuB} > 0$ , red colors). The exact transition line through the space of triad geometries separating the two behaviors is given by  $dL^{BuB}(\alpha)/d\alpha|_{\alpha=0} = 0$ , yielding

$$\log k'/k = \frac{\log k''/k}{1 - \sigma'' k/k''}, \quad (13)$$

which corresponds to the geometries for which the energy and pseudo-invariant solutions collapse (Figure 2(a), black dotted line). Figure 2(b), on the other hand, shows that  $G_3^{BBu}$  and  $G_4^{BBu}$  interactions always conserve an enstrophy-like quantity ( $\alpha^{BBu} > 0$ ) regardless of triad geometry, suggesting they should contribute with an inverse transfer of energy.

We have thus arrived at several testable predictions for the contributions to the total transfer of energy from the four individual MTI components: (i)  $G_i^{uBB}$  triads contribute to a forward transfer (for all sign groups  $i = 1, 2, 3, 4$ ), (ii)  $G_1^{BuB}$  and  $G_4^{BuB}$  contribute to a forward transfer while  $G_2^{BuB}$  and  $G_3^{BuB}$  may contribute either to a forward or inverse transfer depending on triad geometry, and (iii)  $G_1^{BBu}$  and  $G_2^{BBu}$  contribute to a forward transfer while  $G_3^{BBu}$  and  $G_4^{BBu}$  contribute inversely.

### 3.1. Associated Energy Transfer Processes

It is intriguing to note that  $G_3^{BBu}$  and  $G_4^{BBu}$  interactions might be associated with an inverse transfer of magnetic energy since both the smallest and middle triad legs (largest and middle scale) are magnetic components. Because the large-scale magnetic components are of the same helical sign, a connection to the transfer of magnetic helicity is conceivable. Or, put differently: given a transfer of magnetic helicity (e.g., cascade), triad interactions  $G_3^{BBu}$  and  $G_4^{BBu}$  might contribute inversely because they permit an upscale transfer of the magnetic energy associated with each helical sign due to enstrophy-like conservations (Figure 2(c), right-hand side). Indeed, this behavior has already been suggested by Linkmann et al. (2016) and Linkmann & Dallas (2017), who studied the stability properties of (7) given a steady solution for the magnetic field subject to velocity and magnetic perturbations. Note that the transfers between triad legs as indicated by the colored arrows in Figure 2(c) follow from Linkmann et al. (2016).

In their work, Linkmann et al. (2016, 2017), and Linkmann & Dallas (2017) furthermore considered the stability properties of a steady solution for the velocity field subject to velocity and magnetic perturbations. In this case, contributions to the evolution of the magnetic field components comes from the velocity field, which they associated with dynamo action. Several triad interactions were identified which may facilitate both small- and large-scale growth of magnetic field components, thus allowing the operation of small- and large-scale dynamos to be understood at the level of triad interactions. Specifically, it was found that  $G_2^{BuB}$  and  $G_3^{BuB}$  interactions (Figure 2(c), left-hand side) in the limit of nonlocal triad geometries ( $k \ll k' \approx k''$ ) might contribute to large-scale magnetic field growth by large-scale dynamo action, which we find is supported by the nonlocal dependence on triad geometry of the pseudo-invariant (Figure 2(a)). (A discussion of the scale locality of interactions is deferred to Section 6.4.)

On this matter, Linkmann et al. (2016) noted that  $G_2^{BuB}$  triads may produce a helical signature reminiscent of a large-scale  $\alpha$ -dynamo; that is, allowing for the production of large- and small-scale magnetic helicity of opposite signs from a helical velocity field such that the signs of the small-scale kinetic and magnetic helicity match (Brandenburg & Subramanian 2005). Indeed, numerical simulations have since found evidence to support this identification (Linkmann & Dallas 2017). If further combined with the small-scale dynamo process associated with

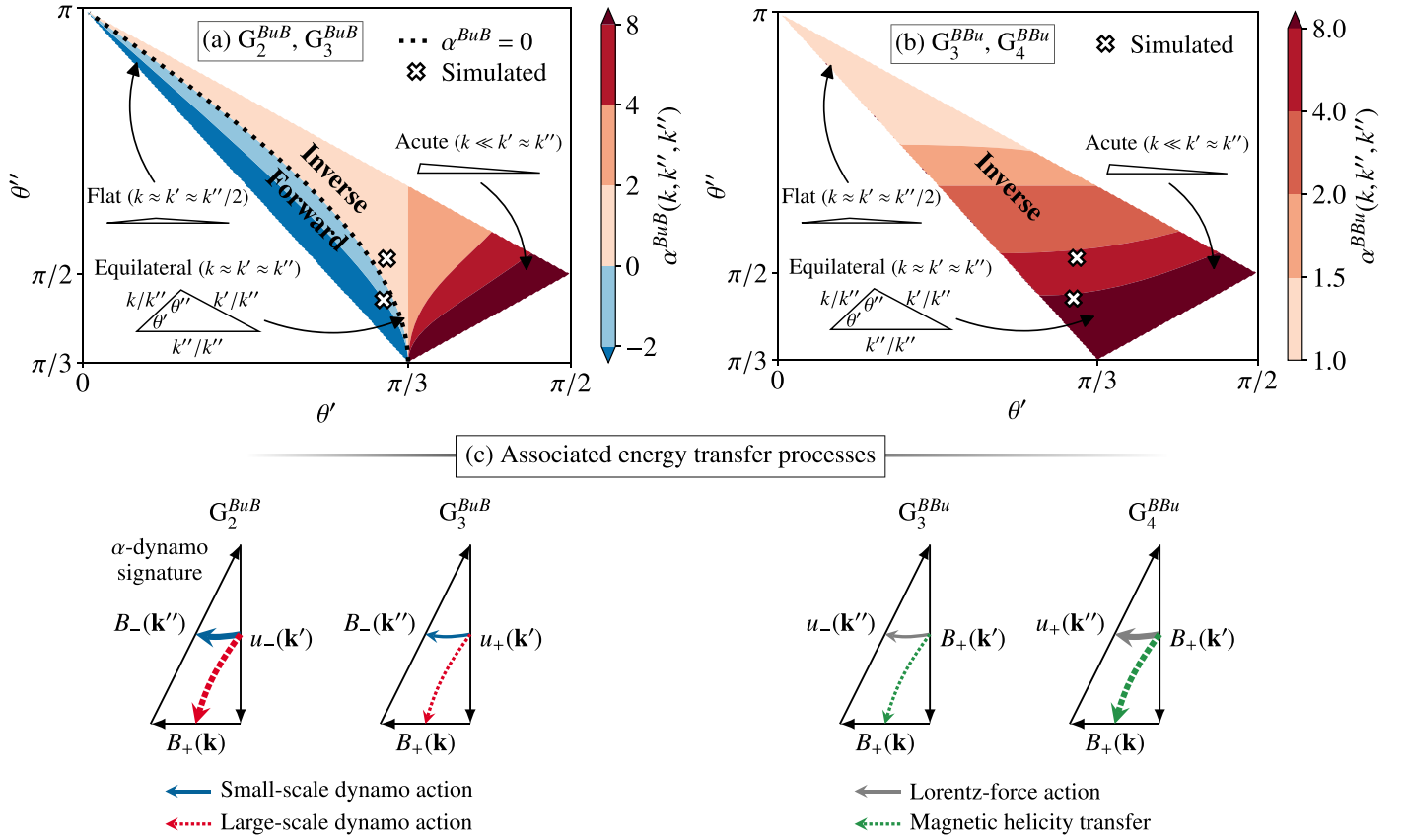


**Figure 2.** Helical triad interactions conserving enstrophy-like pseudo-invariants. The behaviors of triad interactions  $G_2^{BuB}$  and  $G_3^{BuB}$  (panel (a)), and interactions  $G_3^{BBu}$  and  $G_4^{BBu}$  (panel (b)) are proposed to be explained by the conservation of the pseudo-invariant,  $E^{(\alpha)}$ , which depends on triad geometry. Panels (a) and (b) show in red colors the subset of triad geometries conserving an enstrophy-like pseudo-invariant (exponents  $\alpha^{BuB}(k, k', k'') > 0$  and  $\alpha^{BBu}(k, k', k'') > 0$ ), which are conjectured to contribute to an inverse transfer of energy. The black dotted line in panel (a) shows the analytical line partitioning interaction space into the triads that conserve enstrophy-like quantities and those that do not (Equation (13)). Crosses in panels (a) and (b) mark the triad geometries considered in numerical simulations. Panel (c) shows the associated energy transfer processes as identified from a linear stability analysis of (7) (Linkmann et al. 2016; Linkmann & Dallas 2017): dashed arrows represent upscale transfer processes while solid arrows represent downscale transfer processes; thick and thin arrows represent the dominant and subordinate transfers, respectively.

$G_1^{uBB}$  (Linkmann et al. 2017)—for which small-scale magnetic field components are amplified if their helicity matches that of the flow—the dynamo processes facilitated by  $G_2^{BuB}$  triads may produce a helical signature compatible with the stretch–twist–fold dynamo (Vainshtein & Zel’Dovich 1972; Moffatt 1989; Childress & Gilbert 1995; Mininni 2011) as pointed out by Linkmann et al. (2016) and Linkmann et al. (2017). Note that the small-scale dynamo process associated with  $G_1^{uBB}$  triads (and  $G_3^{uBB}$ ) identified by Linkmann et al. (2017) is not at odds with the nonexistence of  $G_i^{uBB}$  pseudo-invariants since a forward energy transfer is implied in that case.

#### 4. The MTI Shell Model

To test the predictions based on the pseudo-invariants, we constructed an MTI shell model (reduced wave-space model). Shell models have previously provided valuable insight into the spectral dynamics of MHD turbulence (Lessinnes et al. 2009; Plunian et al. 2013), and are especially convenient in MHD turbulence due to the added number of nonlinear interactions (Figure 1) making direct numerical simulations computationally expensive. Only relatively recently have direct numerical simulations of (5), (6) been conducted giving some insight into the behavior of helical MHD triad dynamics and the role of the

ideal MHD invariants in the spectral–helical basis (Linkmann et al. 2017) (see Section 6).

Shell models allow simulating very long inertial–inductive ranges at the expense of severely truncating spectral space: only wavenumbers distributed exponentially according to  $k_n = k_0 \lambda^n$  are retained, where  $n = 0, \dots, N$  are the shell indices,  $k_0 \in \mathbb{R}_+$ , and  $\lambda \in ]1, (1 + \sqrt{5})/2] = ]1, \varphi]$ . The golden ratio  $\varphi$  is the upper limit such that any set of nearest-neighbor waves fulfils the triangle inequality as required by (5), (6). All spectral components are generally reduced to depend only on wave magnitudes expect for a few cases (Gürçan 2017, 2018; Monthus 2018), and shell models may therefore be regarded as simple, structureless cascade models.

The pioneering work on constructing helical shell models was done by Benzi et al. (1996) which has since inspired other helical shell models and led to important insights on helically decomposed triad dynamics of HD turbulence (Ditlevsen & Giuliani 2001a, 2001b; Lessinnes et al. 2011; De Pietro et al. 2015, 2017; Rathmann & Ditlevsen 2016; Sahoo et al. 2017b) and MHD turbulence (Lessinnes et al. 2009; Plunian et al. 2013; Stepanov et al. 2015). Following Rathmann & Ditlevsen (2016) for the Navier–Stokes Equations, (5), (6) may similarly be cast into a shell model by noting that the triadic interaction structure is similar but with different interaction coefficients. Considering only homochiral MTIs (elaborated on below) with

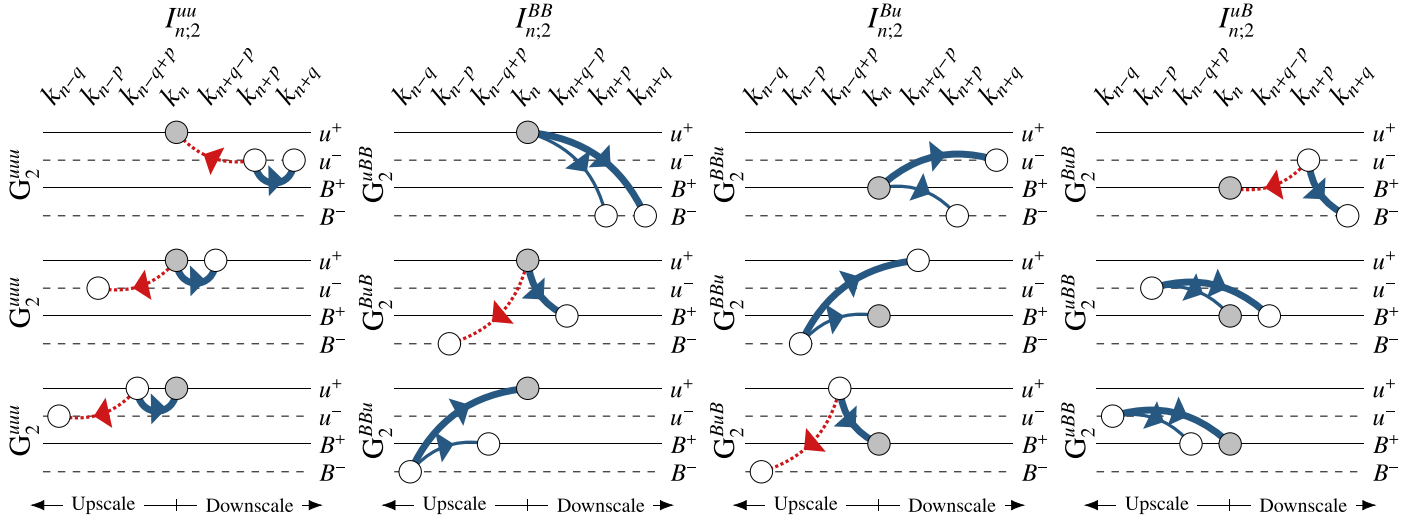


**Figure 3.** Helical triad interactions per shell model term  $I_{n,i}^{uu}$ ,  $I_{n,i}^{BB}$ ,  $I_{n,i}^{Bu}$ , and  $I_{n,i}^{uB}$  for sign group  $i = 2$ . Only interactions coupling to  $u_n^+$  or  $B_n^+$  (filled gray circles) are shown; complementary interactions coupling to  $u_n^-$  or  $B_n^-$  are given by similar but sign-flipped interactions. While the terms  $I_{n,i}^{BB}$ ,  $I_{n,i}^{Bu}$ , and  $I_{n,i}^{uB}$  each contain a mix of the three velocity–magnetic triads ( $G_i^{uBB}$ ,  $G_i^{BuB}$ , and  $G_i^{BBu}$ ), the term  $I_{n,i}^{uu}$  contains only velocity triads ( $G_i^{uuu}$ ). Arrows indicate the average energy transfer directions predicted from the pseudo-invariant observations combined with (7) (fixing the relative leg-to-leg transfer magnitudes): solid blue (dashed red) arrows denote forward (inverse) energy transfers, while thick (thin) arrows represent dominant (subordinate) transfers. Note that the behaviors of  $G_2^{uuu}$  and  $G_2^{BuB}$  interactions are shown assuming local triad geometries (dominant forward transfers).

fixed shape triads (fixed interior angles) and adopting the usual shorthand notation  $u_n^s = u_s(k_n)$  and  $B_n^s = B_s(k_n)$ , the shell model for a single kind of MTI is given by

$$(d_i + D_n^u)u_n^s = sk_n \left[ I_{n,i}^{uu} \left( 1, \frac{\epsilon_i}{\lambda^p}, \frac{\xi_i}{\lambda^q} \right) - I_{n,i}^{BB} \left( 1, \frac{\epsilon_i}{\lambda^p}, \frac{\xi_i}{\lambda^q} \right) \right] + f_n^{u^s} \quad (14)$$

$$(d_i + D_n^B)B_n^s = sk_n [I_{n,i}^{Bu}(\tau_i, \tau_i, \tau_i) - I_{n,i}^{uB}(\tau_i, \tau_i, \tau_i)] + f_n^{B^s}, \quad (15)$$

where the resolved triad interactions are collected in  $I_{n,i}^{VW}$ , defined as

$$I_{n,i}^{VW}(a, b, c) = aV_{n+p}^{s's_i''*}W_{n+q}^{s's_i''} - bV_{n-p}^{s's_i''*}W_{n-p+q}^{s's_i''} + cV_{n-q}^{s's_i''}W_{n-q+p}^{s's_i''}$$

Here, the helical signs of each sign group are for convenience referred to by  $\{s, s', s''\} = \pm\{+, s_i', s_i''\}$ , such that  $\{s_i', s_i''\} = \{-, +\}, \{-, -\}, \{+, -\}, \{+, +\}$  for groups  $i = 1, 2, 3, 4$ , respectively, and the interactions coefficients are given by

$$\begin{aligned} \epsilon_i &= (1 - s_i''\lambda^q)/(\lambda^p - s_i's_i''\lambda^q) \\ \xi_i &= -s_i''(1 - s_i'\epsilon_i) \\ \tau_i &= 1/(s_i'\lambda^p - s_i''\lambda^q). \end{aligned}$$

The integers  $\{p, q\}$  can be related to any triangular shape through the sine rule. The possible resolved triad shapes depend therefore on the combination of  $\{\lambda, p, q\}$ : For  $\lambda \rightarrow 1$  any triad geometry may be constructed for large/small enough values of  $\{p, q\}$ , while for  $\{\lambda, p, q\} = \{\varphi, 1, 2\}$  triads collapse to a line. Hence, for each chosen set of  $\{\lambda, p, q\}$ , the shell model consists, independently of scale  $k_n$ , only of fixed-shape triad interactions. The outer sums over all triad shapes in (5), (6) are thus reduced to just three (fixed-shape) helical triad interactions per MTI component per resolved scale

$k_n$ , exemplified in Figure 3 for the case of  $i = 2$ . Note that only  $I_{n,i}^{uu}$  contains triad interactions of one MTI component exclusively, namely  $G_i^{uuu}$ . The remaining three ( $I_{n,i}^{BB}$ ,  $I_{n,i}^{uB}$ , and  $I_{n,i}^{Bu}$ ) contain a mix of the velocity–magnetic triads  $G_i^{uBB}$ ,  $G_i^{BuB}$ , and  $G_i^{BBu}$ .

The dissipation terms are defined as  $D_n^u = \nu k_n^2 + \nu_L k_n^{-4}$  and  $D_n^B = \eta k_n^2 + \eta_L k_n^{-4}$  where the drag terms,  $\nu_L k_n^{-4}$  and  $\eta_L k_n^{-4}$ , are added in the usual way to remove energy building up at large scales.

Like the ideal MHD Equations (5), (6), the MTI shell model also inviscidly conserves energy ( $E$ ), magnetic helicity ( $H_m$ ), and cross-helicity ( $H_c$ ), which can be shown by applying (14), (15) to (2)–(4), telescoping sums, and inserting the boundary conditions  $u_n^s, B_n^s = 0$  for  $n < 0$  and  $n > N$ . Unlike the ideal MHD Equations (5), (6), however, the MTI shell model (14), (15) conserves all MHD invariants only if the resolved MTIs are homochiral; that is, each MTI component must share the same sign group,  $i$ . Hence, the four possible shell model MTIs are  $G_i^{uuu} + G_i^{uBB} + G_i^{BuB} + G_i^{BBu}$  for  $i = 1, 2, 3, 4$ .

#### 4.1. Forcing Mechanism

The velocity ( $f_n^{u^s}$ ) and magnetic ( $f_n^{B^s}$ ) forcing terms may be constructed to allow full control over the pumping of energy ( $\varepsilon = \varepsilon^u + \varepsilon^B$ ), kinetic helicity ( $\delta^u$ ), magnetic helicity ( $\delta^B$ ), and cross-helicity ( $\gamma = \gamma^u + \gamma^B$ ), where the superscripts  $u$  and  $B$  refer to the injection fields. For the kinetic forcing term, this amounts to solving the forcing balance equations  $\varepsilon^u = f_n^{u^+} u_n^{+,*} + f_n^{u^-} u_n^{-,*} + \text{c.c.}$ ,  $\delta^u = k_n(f_n^{u^+} u_n^{+,*} - f_n^{u^-} u_n^{-,*} + \text{c.c.})$ ,  $\gamma^u = f_n^{u^+} B_n^{+,*} + f_n^{u^-} B_n^{-,*} + \text{c.c.}$ , and  $0 = f_n^{u^+} B_n^{+,*} - f_n^{u^-} B_n^{-,*} + \text{c.c.}$ . For the magnetic forcing term, the balance equations are similar but with  $u$  and  $B$  interchanged, and with the balance of magnetic helicity being given by  $\delta^B = k_n^{-1}(f_n^{B^+} B_n^{+,*} - f_n^{B^-} B_n^{-,*} + \text{c.c.})$ . Solving these closed sets of equations, the mechanical–electromagnetic helical

forcing becomes

$$f_n^{u^s} = \frac{1}{2} \frac{(\varepsilon^u + s\delta^u/k_n)B_n^s - \gamma^u u_n^s}{u_n^{s,*}B_n^s - u_n^s B_n^{s,*}},$$

$$f_n^{B^s} = \frac{1}{2} \frac{(\varepsilon^B + s\delta^B/k_n)u_n^s - \gamma^B B_n^s}{B_n^{s,*}u_n^s - B_n^s u_n^{s,*}},$$

which provides a constant pumping of energy, kinetic helicity, magnetic helicity, and cross-helicity, for constant  $\varepsilon$ ,  $\delta^u$ ,  $\delta^B$ , and  $\gamma$ , respectively, thus allowing the simulated spectral fluxes to easily be normalized against pumping rates.

#### 4.2. Spectral Energy Flux

The total spectral flux of energy (kinetic+magnetic), carried by a homochiral MTI of sign group  $i$  through the  $k_n$ th scale, is given by  $\Pi_i(k_n) = d_{l|n,l} \sum_{m=0}^n (|u_m^+|^2 + |u_m^-|^2 + |B_m^+|^2 + |B_m^-|^2)$ , where  $d_{l|n,l}$  includes only the nonlinear terms in (14), (15). Decomposing the total flux into the four separate MTI-component contributions, or *partial fluxes*, such that

$$\Pi_i(k_n) = \Pi_i^{uuu}(k_n) + \Pi_i^{uBB}(k_n) + \Pi_i^{BuB}(k_n) + \Pi_i^{BBu}(k_n),$$

requires isolating the terms in (14), (15) corresponding to triad interactions  $G_i^{uuu}$ ,  $G_i^{uBB}$ ,  $G_i^{BuB}$ , and  $G_i^{BBu}$ , which can be shown to give

$$G_i^{uuu} \begin{cases} d_{l|n,l} u_n^s = sk_n I_{n,i}^{uu} \left(1, \frac{\varepsilon_i}{\lambda^p}, \frac{\xi_i}{\lambda^q}\right) \\ d_{l|n,l} B_n^s = 0 \end{cases}$$

$$G_i^{uBB} \begin{cases} d_{l|n,l} u_n^s = -sk_n I_{n,i}^{BB} (1, 0, 0) \\ d_{l|n,l} B_n^s = -sk_n [I_{n,i}^{uB} (0, \tau_i, 0) + I_{n,i}^{uB} (0, 0, \tau_i)] \end{cases}$$

$$G_i^{BuB} \begin{cases} d_{l|n,l} u_n^s = -sk_n I_{n,i}^{BB} \left(0, \frac{\varepsilon_i}{\lambda^p}, 0\right) \\ d_{l|n,l} B_n^s = sk_n [I_{n,i}^{Bu} (0, 0, \tau_i) - I_{n,i}^{uB} (\tau_i, 0, 0)] \end{cases}$$

$$G_i^{BBu} \begin{cases} d_{l|n,l} u_n^s = -sk_n I_{n,i}^{BB} \left(0, 0, \frac{\xi_i}{\lambda^q}\right) \\ d_{l|n,l} B_n^s = sk_n [I_{n,i}^{Bu} (\tau_i, 0, 0) + I_{n,i}^{uB} (0, \tau_i, 0)] \end{cases}.$$

Using these MTI-decomposed equations, the partial fluxes follow as (telescoping sums and applying the boundary conditions  $u_n^s, B_n^s = 0$  for  $n < 0$  and  $n > N$ )

$$\Pi_i^{uuu}(k_n) = + \sum_{m=n+1}^{n+q} \Delta_{m,i}^{uuu} - s' \varepsilon_i \sum_{m=n+1}^{n+q-p} \Delta_{m,i}^{uuu} \quad (16)$$

$$\Pi_i^{uBB}(k_n) = - \sum_{m=n+1}^{n+q} \Delta_{m,i}^{uBB} + s' \lambda^p \tau_i \sum_{m=n+1}^{n+q-p} \Delta_{m,i}^{uBB} \quad (17)$$

$$\Pi_i^{BuB}(k_n) = -\tau_i \sum_{m=n+1}^{n+q} \Delta_{m,i}^{BuB} + s' \varepsilon_i \sum_{m=n+1}^{n+q-p} \Delta_{m,i}^{BuB} \quad (18)$$

$$\Pi_i^{BBu}(k_n) = +\tau_i \sum_{m=n+1}^{n+q} \Delta_{m,i}^{BBu} - s' \lambda^p \tau_i \sum_{m=n+1}^{n+q-p} \Delta_{m,i}^{BBu}, \quad (19)$$

where the triple correlators,  $\Delta_{m,i}^{XYZ}$ , are defined as

$$\Delta_{m,i}^{XYZ} = 2k_{m-q} \text{Re} [X_{m-q}^{+,*} Y_{m-q+p}^{s_i,*} Z_m^{s_i''} - X_{m-q}^{-,*} Y_{m-q+p}^{-s_i,*} Z_m^{-s_i''}].$$

Note that the partial fluxes (16)–(19) are of the total energy (kinetic+magnetic). Thus, in the same way each MTI component separately conserves total energy as follows from

setting  $\alpha = 0$  in (9)–(12), the partial fluxes are based on conservative dynamics. This, however, does not apply to the individual kinetic and magnetic energy flux contributions to the partial fluxes, and the pseudo-invariants are therefore not relevant to them.

## 5. Numerical Results

For each of the four homochiral MTIs, two different triad shapes (crosses in Figure 2) were considered in order to test the partial flux predictions. The model was configured using a shell spacing of  $\lambda = 1.2$  with  $\{p, q\} = \{1, 2\}$  and  $\{p, q\} = \{3, 4\}$ , corresponding to pseudo-invariant exponents of  $\alpha^{BuB} = \{-2.0, +1.0\}$  and  $\alpha^{BBu} = \{+8.8, +4.5\}$ , respectively. The chosen triad geometries thus sample contributions from both the forward and inverse parts of  $G_i^{BuB}$  interaction space (Figure 2(a)).

For simplicity, all model simulations were configured with identical free parameters (the values of which were found not to influence results):  $\nu = \mu = 1 \times 10^{-8}$  (i.e., a magnetic Prandtl number of one),  $\nu_L = \mu_L = 1 \times 10^1$ ,  $k_0 = 1$ , and  $N = 76$ . The modes  $u_n^s$  and  $B_n^s$  were initialized in a K41-scaling state  $\sim k_n^{-2/3}$  (the shell model equivalent of  $\sim k^{-5/3}$ ) with zero helicity of any kind, and stepped forward using a fourth-order Runge–Kutta integration scheme with a time-step of  $\Delta t = 5 \times 10^{-7}$ . The injection rates  $\varepsilon^u = \varepsilon^B = 1/2$ , and  $\delta^u, \delta^B, \gamma = 0$  (i.e., no forcing handedness, elaborated on in the discussion) were evenly applied over  $p$  shells, starting from shell  $n_f = 30$ . Thus, in the  $p = 3$  configuration, shells #31 and #32 were also forced. Note that while dynamo studies typically inject only kinetic energy, both kinetic and magnetic energy were injected in the present simulations. Although no difference in the energy flux partitioning between MTI components was found for homochiral MTIs  $i = 1, 2, 3$ , the magnetic field collapsed for  $i = 4$  unless magnetic energy was injected.

The simulated partial energy fluxes within the four homochiral configurations  $i = 1, 2, 3, 4$  are shown in Figures 4(a), (b), (c), and (d), respectively, calculated using (16)–(19). The energy flux partitionings are shown for both triad shapes, labeled in the legends by the corresponding  $\alpha^{BuB}$  exponents. Gray/black lines represent components without pseudo-invariants, whereas components marked by colored lines possess pseudo-invariants: blue colors indicate components for which the pseudo-invariant exponents are negative ( $\alpha < 0$ , hypothesized forward contribution), whereas red/orange colors mark components conserving enstrophy-like quantities with positive exponents ( $\alpha > 0$ , hypothesized inverse contribution).

Figures 4(a) and (b) show the partitionings within homochiral MTIs  $i = 1$  and  $i = 2$  conform with the pseudo-invariant predictions: all MTI components contribute to a forward transfer, whereas  $G_2^{BuB}$  (conserving an enstrophy-like quantity,  $\alpha^{BuB} > 0$ ) contributes to an inverse transfer.

Figure 4(c) shows the partitioning within MTI  $i = 3$  almost behaving as expected: all components contribute to a forward transfer of energy, except for  $G_3^{BuB}$  and  $G_3^{BBu}$  interactions which have their behaviors reversed—i.e., components conserving enstrophy-like quantities are found to contribute to a forward energy transfer and vice-versa.

Figure 4(d) shows the partitioning within MTI  $i = 4$  also conforms with predictions: all components contribute to a forward transfer of energy, whereas  $G_4^{BBu}$  (conserving an enstrophy-like quantity,  $\alpha^{BBu} > 0$ ) contributes inversely. For

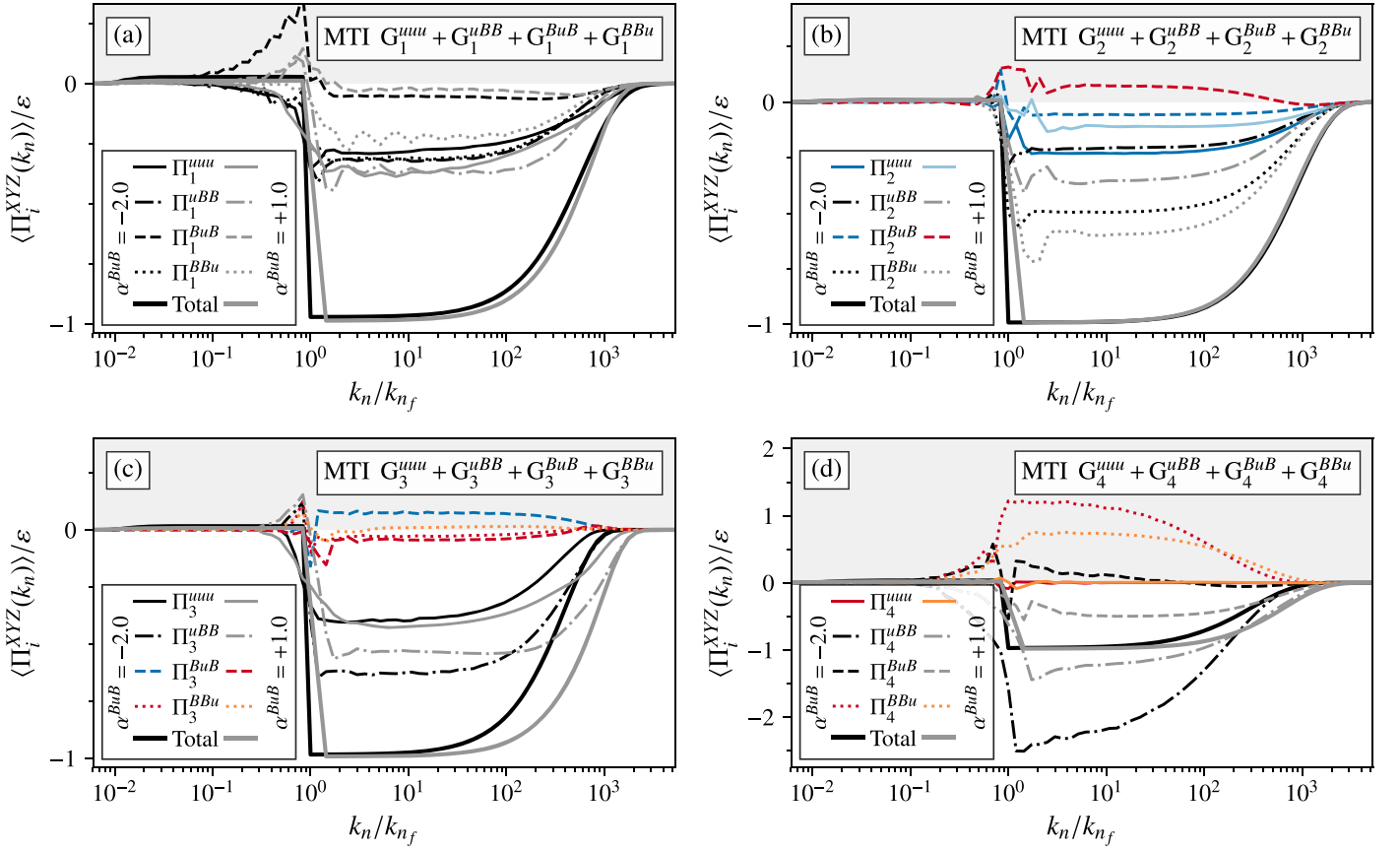


**Figure 4.** Simulated partial energy fluxes associated with each MTI component for each of the four possible homochiral MTIs  $G_i^{uuu} + G_i^{uBB} + G_i^{BuB} + G_i^{BBu}$  ( $i = 1, 2, 3, 4$ ) in panels (a)–(d), respectively. The partial fluxes are calculated using (16)–(19). Negative (positive) values correspond to forward/downscale (inverse/upscale) fluxes. Blue lines denote hypothesized forward contributions according to the pseudo-invariant predictions, while red/orange lines denote hypothesized inverse contributions (interactions conserving an enstrophy-like quantity). Black/gray lines denote contributions by interactions not conserving any pseudo-invariants.

the simulated triad shape corresponding to  $\alpha^{BuB} = -2.0$ , however, the  $G_4^{BuB}$  component carries a small inverse contribution in spite of not conserving any enstrophy-like quantity.

Finally, in the nonlinear regime considered here (non-negligible back-reaction of the Lorentz force on the flow), we note that the partial fluxes are more or less constant, suggesting that relatively local interactions in wave space may facilitate both up- and downscale embedded energy cascades.

## 6. Discussion

The simulated energy flux partitionings between MTI components largely (but not fully) support the proposed influence of the new pseudo-invariants, which allow the energy flux partitionings to be understood in terms of conserved quantities in analogy to enstrophy in 2D HD turbulence. In this section, we further discuss and investigate in detail the relevance of our results to larger triad networks (Section 6.1), the effect of coupling different MTI components and the mismatch between some of the predictions and simulations (Section 6.2), the possibility of instigating an energy transfer reversal by biasing triad interactions (Section 6.3), the scale locality of the triad interactions which may facilitate large-scale  $\alpha$ -dynamo action and the inverse transfer of magnetic helicity (Section 6.4), and caveats about the robustness of our results to various forcing scenarios (Section 6.5).

### 6.1. Relevance to Large Triad Networks

The relevance of the new partial invariants to more realistic triad configurations consisting of large MTI networks may be surmised by comparing with recent direct numerical simulations (DNSs) of (1) or (5), (6). The DNS by Linkmann & Dallas (2017) considered a nonhelical and a positive helical forcing of the velocity and magnetic fields, respectively, thus introducing a dominant sign of magnetic helicity. In this case, both forward and inverse (bidirectional) magnetic helicity cascades were identified, and the inverse component was attributed to (dominant) contributions from  $G_3^{BBu}$  and  $G_4^{BBu}$  triads which involve interactions between magnetic components of the same helical sign (Figure 2(c)). However, in the steady-state regime, low-wavenumber modes were found to develop negative helicity spectra despite a mean positive value due to pumping (and distributed by a cascade process). Because the forcing scenario led to a positive kinetic helicity spectrum (associated with the action of the Lorentz force) the negative helicity spectrum at large scales was argued to be the result of large-scale dynamo action facilitated by  $G_2^{BuB}$  triads, since only the action of such triads was consistent with the simulated helical signature ( $\alpha$ -dynamo signature).

Linkmann et al. (2017) also considered strongly magnetized flows by using a helical magnetic forcing in a DNS of (5), (6). They noted that if the triads that facilitate the inverse transfer of magnetic helicity indeed are the dominant ones from a linear stability analysis, then the transport efficiency depends on the

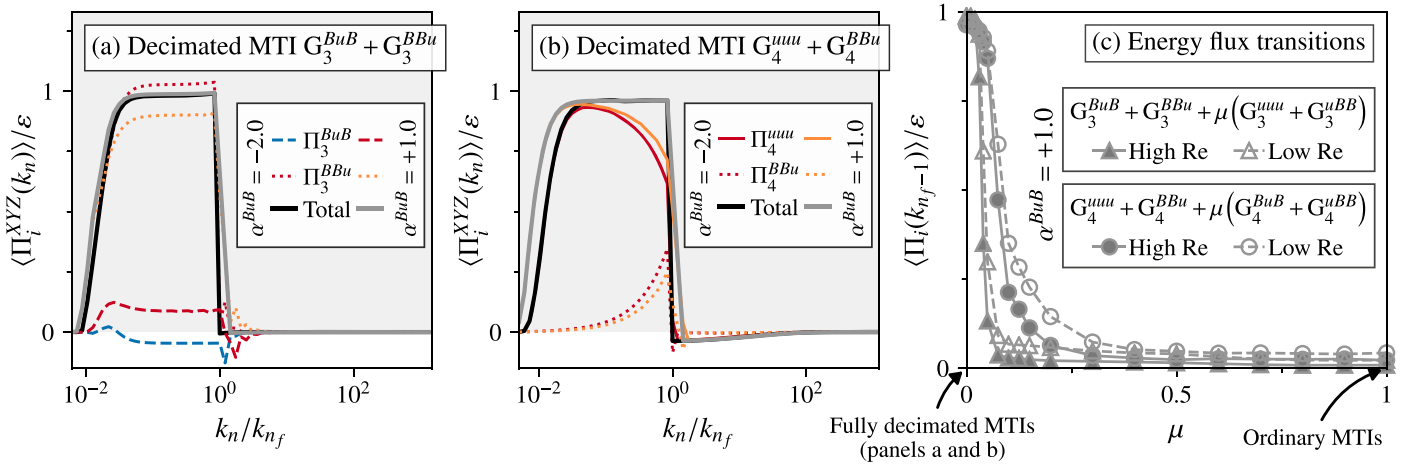


**Figure 5.** Panels (a) and (b): simulated partial energy fluxes associated with each MTI-component of the decimated MTIs  $G_3^{BuB} + G_3^{BBu}$  and  $G_4^{uuu} + G_4^{BBu}$ . Negative (positive) values correspond to forward/downscale (inverse/upscale) fluxes. Blue lines denote hypothesized forward partial fluxes according to the pseudo-invariant predictions, while red/orange lines denote hypothesized inverse partial fluxes (interactions conserving an enstrophy-like quantity). Panel (c): inverse energy flux as a function of the decimation (control) parameter,  $\mu$ , for the two MTIs  $G_3^{BuB} + G_3^{BBu} + \mu(G_3^{uuu} + G_3^{BBu})$  and  $G_4^{uuu} + G_4^{BBu} + \mu(G_4^{BuB} + G_4^{BBu})$ , defined as the total flux magnitude immediately above the forcing scale,  $k_{n_f-1}$ , normalized by the pumping rate,  $\varepsilon$ . Note that the MTIs are fully decimated for  $\mu = 0$  (partitionings shown in panels (a) and (b)), while for  $\mu = 1$  the ordinary MTIs are recovered (partitionings shown in Figures 4(c) and (d)). Filled markers denote high Reynolds number simulations (canonical model configuration used throughout), whereas empty markers denote low Reynolds number simulations (large-scale viscosities increased by a factor of 10).

degree to which small-scale magnetic and kinetic helicity is of the same sign, which they confirmed numerically. Thus, dominant triad interactions which have large growth rates of perturbed modes from a stability analysis, such as  $G_4^{BBu}$ , might play an important role in the transfer of magnetic helicity. Their instability analysis also predicted that triads with helical signatures reminiscent of an  $\alpha$ -type dynamo should be dominant due to large growth rates, which too was confirmed numerically in dynamo experiments using a purely mechanical forcing. Therefore, by similar arguments,  $G_2^{BuB}$  triads might play an important role in large triad networks by facilitating large-scale  $\alpha$ -dynamo action.

In short, the pseudo-invariants may, arguably, have relevance for larger triad networks in the sense that the triads we predict to facilitate inverse energy transfers have previously been suggested important in DNS studies (and triad stability analyses) for large-scale magnetic structure formation by large-scale dynamo action and the inverse transfer of magnetic helicity.

### 6.2. Effect of Coupling MTI Components

The homochiral MTIs of sign groups  $i = 3$  and  $i = 4$  show discrepancies between simulated partial fluxes and predictions based on the pseudo-invariants (Section 5). Interestingly, for the homochiral MTI  $i = 3$ , these discrepancies correspond to triad interactions with low growth rates of the perturbed modes in a linear stability analysis (Linkmann & Dallas 2017) (to be understood why). In the case of the shell model, we find that coupling-induced effects, caused by the coupling of MTI components, might play an important role by altering the component-wise behaviors (partial fluxes) compared to predictions. This is exemplified by considering additional decimated simulations in which only  $G_i^{BuB}$  and  $G_i^{BBu}$  are coupled, i.e., decomposing the MTIs by disregarding  $G_i^{uuu}$  and  $G_i^{uBB}$  interactions. Using the same model configuration as above, Figure 5(a) shows the resulting energy flux partitioning

between the two components  $G_3^{BuB}$  and  $G_3^{BBu}$  in the decimated MTI  $G_3^{BuB} + G_3^{BBu}$ . For all four decimated MTIs  $G_i^{BuB} + G_i^{BBu}$  ( $i = 1, 2, 3, 4$ ), the component-wise partial fluxes are found to conform with the pseudo-invariant predictions ( $i = 1, 2, 4$  not shown), suggesting the discrepancies between the full and decimated MTIs might be due to coupling-induced effects. Whether this is a model artefact or a property also shared by large triad networks (5), (6) is not clear.

### 6.3. Classification of Energy Flux Transitions

Efforts have previously been made to classify how HD and MHD systems may transition from a state in which energy is transferred (e.g., by a cascade process) primarily downscale to primarily upscale as a function of external mechanisms such as rotation, confinement, stratification, and background magnetic fields, and by which triad interaction energy is channeled upscale (see Alexakis & Biferale 2018 for a review). For example, by numerically varying the thickness of a nonconducting fluid layer, a possible critical thickness has been reported at which a continuous but nonsmooth (second order) transition occurs from a forward to inverse energy cascade (Benavides & Alexakis 2017). By considering a nonconducting fluid in a rotating reference frame, Buzdicotti et al. (2018) recently numerically explored the transition from a forward cascade to a split forward–inverse cascade as a function of rotation rate, finding that  $G_4^{uuu}$  HD triad interactions—which conserve enstrophy-like quantities by conserving both signs of kinetic helicity separately—might predominantly be responsible for channelling energy upscale under rapid rotation.

Inverse energy cascades in 3D MHD turbulence, such as found in the presence of strong background (guiding) magnetic fields both numerically (Alexakis 2011) and experimentally (Baker et al. 2018), might also be related to subsets of helical triad interactions conserving enstrophy-like quantities. This is indeed possible in principle as shown in Figure 5(a), which is a robust result for other combinations of enstrophy-like

conserving interactions, such as shown in Figure 5(b) for the decimated MTI  $G_4^{uuu} + G_4^{BBu}$ .

In an attempt to explore whether favoring interactions conserving enstrophy-like quantities can induce a predominantly inverse transfer of energy in MHD turbulence, we conducted a set of triad-biasing (decimation) experiments inspired by Sahoo et al. (2015, 2017a, 2017b) and Sahoo & Biferale (2015). Specifically, we considered the decimation of the two homochiral MTIs  $i = 3$  and  $i = 4$  using a control parameter,  $\mu$ , such that only enstrophy-like conserving interactions are considered for  $\mu = 0$  (corresponding partitionings shown in Figures 5(a) and (b)) while all interactions are considered without bias for  $\mu = 1$  (corresponding partitionings shown in Figures 4(c) and (d)), that is

$$G_3^{BuB} + G_3^{BBu} + \mu(G_3^{uuu} + G_3^{uBB}) \quad (20)$$

$$G_4^{uuu} + G_4^{BBu} + \mu(G_4^{BuB} + G_4^{uBB}). \quad (21)$$

Figure 5(c) shows the resulting total inverse energy flux immediately above the forcing scale,  $k_{n-1}$ , as a function of  $\mu$  for the two decimated MTIs (20) (triangles) and (21) (circles) with triad shapes corresponding to  $\alpha^{BuB} = +1.0$ . Following the terminology in Alexakis & Biferale (2018), we find that the cascade transitions are continuous and smooth from strictly forward to strictly inverse, but might tend toward discontinuous (first-order) transitions in the limit of long inertial–inductive ranges (difference in Figure 5(c) between full markers (high Reynolds number, canonical model configuration) and empty markers (low Reynolds number, large-scale viscosities increased by a factor of 10)).

Sahoo et al. (2017a) recently studied the decimated HD system  $\mu(G_1^{uuu} + G_2^{uuu} + G_3^{uuu}) + G_4^{uuu}$ , finding also that the transition toward an inverse energy cascade as a function of  $\mu$  becomes a discontinuous jump in the limit of large Reynolds number. In addition, they found that the transition appears to be quasi singular in the sense that the critical control parameter value is close to  $\mu = 1$ . Here, we find that this result also carries over to MHD systems, suggesting that enstrophy-like conserving interactions are comparatively less efficient at transferring energy, and thus only a small percentage of forward-transferring interactions are necessary to maintain a predominantly forward transfer of energy.

#### 6.4. Scale Locality of Interactions

In HD turbulence, the relative importance of local versus nonlocal triad interactions has been vigorously investigated both theoretically and numerically. Although numerical simulations have demonstrated that nonlocal interactions involving large-scale flow components can influence the energy cascade (Domaradzki & Rogallo 1990; Alexakis et al. 2005a; Mininni et al. 2006), thus challenging to the Kolmogorov picture of a local energy cascade, other numerical studies considering high Reynolds number flows (Domaradzki & Carati 2007; Mininni et al. 2008; Domaradzki et al. 2009) and theoretical considerations (Aluie & Eyink 2009; Eyink & Aluie 2009) suggest that nonlocal contributions to the energy cascade are significantly smaller than local contributions. Thus, while individual nonlocal interactions (having one leg at the energy-containing scales) may contribute more to the energy flux than individual local interactions, the act of summing over

all triad contributions is dominated by local interactions (Domaradzki & Carati 2007).

In the MHD case, the picture is less clear, but there is a growing consensus—at least for intermediate Reynolds numbers—that MHD turbulence is less local than HD turbulence (Mininni 2011). Depending on the flow configuration (forced, decaying, presence of external fields), nonlocal transfers have been found in MHD turbulence which involve interactions between velocity and magnetic fields (Alexakis et al. 2005b; Brandenburg & Subramanian 2005; Verma et al. 2005; Carati et al. 2006), or related to the transfer of magnetic helicity (Alexakis et al. 2006; Aluie & Eyink 2010), while velocity–velocity and magnetic–magnetic field interactions are mostly local (Mininni 2011).

The possible relevance of the pseudo-invariants for transfer processes in MHD turbulence depends, therefore, on the degree to which the aggregate of triads conserving them are relevant for the velocity and magnetic field evolutions. Since the HD interactions  $G_2^{uuu}$  conserve enstrophy-like invariants only in the nonlocal limit, their relevance is arguably small insofar as HD flows are dominated by local interactions. We note, however, that the flow configuration (e.g., aspect ratio, rotation) might influence which triads are predominantly responsible for channelling energy (Alexakis & Biferale 2018), suggesting care must be taken when determining the relative importance of triads. Conversely, in the case of MHD turbulence, the enstrophy-like conservations are found in both the local and nonlocal (acute triad) parts of interaction space and for both pseudo-invariants (red colors in Figures 2(a) and (b)).

Whether the pseudo-invariants are relevant only for constraining cascade contributions to the total energy flux, or more generally applicable to spectral transfers (processes not associated with a constant flux), is an open question. We note, however, that the enstrophy-like conservation by  $G_3^{BBu}$  and  $G_4^{BBu}$  triads, which have magnetic components of like-signed helicity as the two smallest triad legs (largest scales), supports the possibility of an inverse magnetic energy transfer consistent with an inverse magnetic helicity cascade, as pointed out by Linkmann et al. (2016) and Linkmann & Dallas (2017). The inter-scale transfer of magnetic helicity is complex, with concurrent forward and inverse contributions (Mininni 2011; Linkmann & Dallas 2017). On this matter, it is not clear whether the inverse component (and accompanied energy transfers) is dominated by local or nonlocal transfers (Alexakis et al. 2006; Aluie & Eyink 2010; Mininni 2011; Müller et al. 2012; Linkmann & Dallas 2016; Linkmann et al. 2017). Unfortunately, this work provides no further clarity since the dependence of the pseudo-invariant on triad geometry is consistent with both local and nonlocal magnetic helicity transfers being possible. We do, however, find that local transfers can take the form of a (constant flux) cascade process.

If the pseudo-invariants are indeed generally applicable to spectral transfers, the agreement is intriguing between the (triadic) large-scale dynamo action suggested to be facilitated by  $G_2^{BuB}$  and  $G_3^{BuB}$  triads in the nonlocal limit ( $k \ll k' \approx k''$ ) (Linkmann et al. 2016, 2017) and the enstrophy-like conservations. Of the two,  $G_2^{BuB}$  interactions have the same helical signature as the  $\alpha$ -effect (Linkmann et al. 2016), and have stability properties suggesting a dominant role over  $G_3^{BuB}$  interactions. Although care must be taken when extrapolating the behavior of single triads to a large system of triads (Moffatt 2014), we note that the enstrophy-like conservation by

$G_2^{BuB}$  (and  $G_3^{BuB}$ ) (Figure 2(a)) suggests that inverse transfers from such triads might be dominated by nonlocal interactions compared to  $G_3^{BBu}$  and  $G_4^{BBu}$  triads (Figure 2(b)); that is, the inverse transfer of magnetic helicity is more local than large-scale  $\alpha$ -dynamo action.

### 6.5. Universality of Energy Flux Partitioning

The partitioning of the energy cascade between symmetrized helical triad interactions was recently investigated by Alexakis (2017) in a direct numerical simulation of the spectral–helical Navier–Stokes equation. Like here, it was found that the energy cascade partitions itself into approximately constant partial-flux components within the inertial range, an intriguing result given that only the total energy flux is required to be constant. Moreover, Alexakis (2017) found that the partitioning was unaffected by the pumping of kinetic helicity, suggesting the partitioning might be universal (among a given set of resolved triads). If so, the physical explanation for the directionalities of the partial fluxes in terms of pseudo-invariants might be applicable in a general, forcing-independent sense.

Inspired by this result, we conducted additional simulations where the four homochiral MTIs were forced with kinetic helicity ( $\delta^u$ ), magnetic helicity ( $\delta^B$ ), and cross-helicity ( $\gamma$ ) besides energy, in contrast to the nonhelical forcing used above ( $\delta^u, \delta^B, \gamma = 0$ ). While the partitionings were found to be independent of  $\delta^u$  and  $\delta^B$ , suggesting the partitionings might be universal, the same was not found for a nonzero injection of cross-helicity ( $\gamma \neq 0$ ). This is exemplified in Figure 6 for the homochiral MTI  $i = 1$  (similar results were found for  $i = 2, 3, 4$ ), demonstrating the divergent, non-constant partial fluxes which develop in the case of  $\gamma^u = 0.25$ . In addition, when pumping cross-helicity, the simulated directionalities of the partial fluxes generally do not agree with the pseudo-invariant predictions: in Figure 6, all components are predicted to contribute to a forward energy transfer since no enstrophy-like quantities are conserved.

Because the evolution of magnetic modes depends on the alignment between velocity and magnetic modes (cross-helicity) according to (6), it is not entirely surprising that injecting cross-helicity can affect the detailed partitioning. Note that this result is in agreement with a linear stability analysis which also predicts that triad leg (modal) stabilities depend on velocity–magnetic alignments (Linkmann et al. 2016).

The present analysis considered only a magnetic Prandtl number of one. While investigating large and small magnetic Prandtl number flows is out of scope of the present work, studies such as Verma & Kumar (2016) indicate that under some forcing conditions the partitioning might be unaffected, although helically decomposed dynamics were not considered in that case.

## 7. Conclusion

In conclusion, we identified new, partially conserved quantities among the elementary three-wave (triad) interactions in spectral–helically decomposed ideal MHD turbulence. Because the new quantities conserved by a subset of triad interactions are enstrophy-like, we conjecture that such interactions might contribute to embedded, inverse energy transfers developing in 3D MHD turbulence in analogy to enstrophy-conserving triad interactions in 2D HD turbulence.

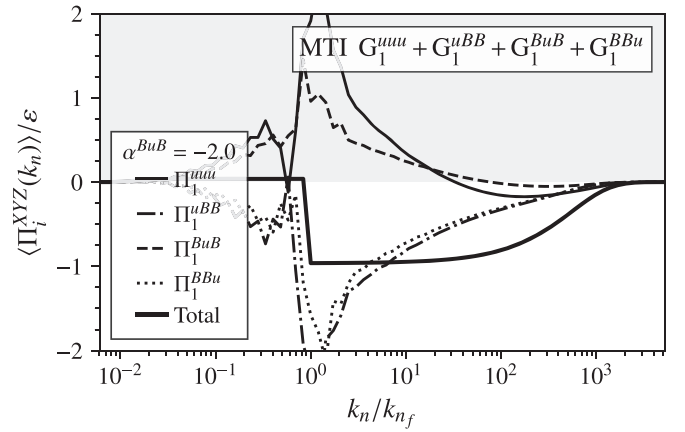


**Figure 6.** Simulated energy flux partitioning between the four MTI components within the homochiral MTI  $G_1^{uuu} + G_1^{uBB} + G_1^{BuB} + G_1^{BBu}$  for a nonzero cross-helicity pumping of  $\gamma^u = 0.25$ . Negative (positive) values correspond to forward/downscale (inverse/upscale) fluxes.

Among the enstrophy-like conserving interactions are the helical interactions recently identified with facilitating large-scale  $\alpha$ -dynamo action ( $G_2^{BuB}$ ) and the inverse (upscale) transfer of magnetic helicity ( $G_4^{BBu}$ ) (Figure 2(c)). The partial invariants (pseudo-invariants) might therefore play an important role in the understanding of which physical mechanisms are behind the transfer processes leading to large-scale magnetic structure formation, and therefore of astrophysical interest. Importantly, the conservation of the pseudo-invariants depends on the scale locality of the triad interactions (Figures 2(a) and (b)). Based on this, we conjecture that large-scale dynamo action with an  $\alpha$ -type helical signature (large- and small-scale magnetic field components having opposite signs of helicity) is a transfer process that is more nonlocal in wave space than the inverse transfer of magnetic helicity, insofar as they are facilitated by  $G_2^{BuB}$  and  $G_4^{BBu}$  triads, respectively.

In order to test the predictions based on the new pseudo-invariants, we introduced a helically decomposed reduced wave-space model (shell model). By conducting numerical simulations of the four kinds of homochiral minimal sets of triad interactions (MTIs; minimal in the sense of being required to conserve the ideal MHD invariants), we demonstrated the usefulness of the partial invariants for understanding the resulting embedded energy flux contributions (partial fluxes) from the triadic components constituting an MTI. Inspired by recent HD studies showing that the relative importance of different triad interactions might depend on flow configuration (e.g., rotation or confinement), we additionally demonstrated the possibility of strictly inverse transfers of energy developing if enstrophy-like conserving interactions are favored, finding that only a small percentage of triads not conserving enstrophy-like quantities are necessary to maintain a dominant downscale transfer of energy (magnetic+kinetic).

While for simplicity this study concerned itself with the case of a magnetic Prandtl number of one, we find that the embedded partial fluxes are generally constant over inertial–inductive ranges, indicating that forward and inverse energy cascades might generally exist embedded in MHD turbulence. Importantly, however, we note that the injection of cross-helicity by the forcing mechanism, and the effect of coupling certain types of MTI components (triad interactions),

demonstrate cases where the directions of the simulated partial fluxes do not agree with the pseudo-invariant predictions. Whether this is a model artefact or a property shared by more comprehensive (and thus more realistic) large triad networks as represented by the spectral-helicity decomposed MHD Equations (5), (6), is not clear.

The authors thank the anonymous referee for useful comments and references that led to an appreciably improved manuscript which, importantly, includes the connection between the (triadic)  $\alpha$ -dynamo and the  $G_2^{BuB}$  pseudo-invariant, and Luca Biferale for comments and suggestions leading to Section 6.3.

### ORCID iDs

Nicholas M. Rathmann  <https://orcid.org/0000-0001-7140-0931>

Peter D. Ditlevsen  <https://orcid.org/0000-0003-2120-7732>

### References

- Alexakis, A. 2011, *PhRvE*, **84**, 056330  
 Alexakis, A. 2017, *JFM*, **812**, 752  
 Alexakis, A., & Biferale, L. 2018, *PhR*, **767**, 1  
 Alexakis, A., Mininni, P., & Pouquet, A. 2005a, *PhRvL*, **95**, 264503  
 Alexakis, A., Mininni, P. D., & Pouquet, A. 2005b, *PhRvE*, **72**, 046301  
 Alexakis, A., Mininni, P. D., & Pouquet, A. 2006, *ApJ*, **640**, 335  
 Aluie, H. 2017, *NJPh*, **19**, 025008  
 Aluie, H., & Eyink, G. L. 2009, *PhFl*, **21**, 115108  
 Aluie, H., & Eyink, G. L. 2010, *PhRvL*, **104**, 081101  
 Baker, N. T., Pothérat, A., Davoust, L., & Debray, F. 2018, *PhRvL*, **120**, 224502  
 Benavides, S. J., & Alexakis, A. 2017, *JFM*, **822**, 364  
 Benzi, R., Biferale, L., Kerr, R., & Trovatore, E. 1996, *PhRvE*, **53**, 3541  
 Bian, X., & Aluie, H. 2019, *PhRvL*, **122**, 135101  
 Biferale, L., Musacchio, S., & Toschi, F. 2012, *PhRvL*, **108**, 164501  
 Biskamp, D. 1993, *Nonlinear Magnetohydrodynamics* (Cambridge: Cambridge Univ. Press)  
 Blackman, E. G. 2016, *Multi-scale Structure Formation and Dynamics in Cosmic Plasmas* (Berlin: Springer), 59  
 Boffetta, G., & Musacchio, S. 2010, *PhRvE*, **82**, 016307  
 Brandenburg, A. 2001, *ApJ*, **550**, 824  
 Brandenburg, A., Kahnishvili, T., & Tevzadze, A. G. 2015, *PhRvL*, **114**, 075001  
 Brandenburg, A., & Subramanian, K. 2005, *PhR*, **417**, 1  
 Brissaud, A., Frisch, U., Léorat, J., Lesieur, M., & Mazure, A. 1973, *PhFl*, **16**, 1366  
 Brun, A. S., & Browning, M. K. 2017, *LRSP*, **14**, 4  
 Buzzicotti, M., Aluie, H., Biferale, L., & Linkmann, M. 2018, *PhRvF*, **3**, 034802  
 Carati, D., Debliquy, O., Knaepen, B., Teaca, B., & Verma, M. 2006, *JTurb*, **7**, 51  
 Childress, S., & Gilbert, A. D. 1995, *Stretch, Twist, Fold: the Fast Dynamo*, Vol. 31 (Berlin: Springer Science & Business Media)  
 Constantin, P., & Majda, A. 1988, *CMaPh*, **115**, 435  
 De Pietro, M., Biferale, L., & Mailybaev, A. A. 2015, *PhRvE*, **92**, 043021  
 De Pietro, M., Mailybaev, A. A., & Biferale, L. 2017, *PhRvF*, **2**, 034606  
 Démoulin, P. 2007, *AdSpR*, **39**, 1674  
 Ditlevsen, P. D., & Giuliani, P. 2001a, *PhFl*, **13**, 3508  
 Ditlevsen, P. D., & Giuliani, P. 2001b, *PhRvE*, **63**, 036304  
 Domaradzki, J. A., & Carati, D. 2007, *PhFl*, **19**, 085112  
 Domaradzki, J. A., & Rogallo, R. S. 1990, *PhFl*, **2**, 413  
 Domaradzki, J. A., Teaca, B., & Carati, D. 2009, *PhFl*, **21**, 025106  
 Eyink, G. L., & Aluie, H. 2009, *PhFl*, **21**, 115107  
 Frisch, U., Pouquet, A., Léorat, J., & Mazure, A. 1975, *JFM*, **68**, 769  
 Gürçan, Ö. 2017, *PhRvE*, **95**, 063102  
 Gürçan, Ö. 2018, *PhRvE*, **97**, 063111  
 Hood, A. W., & Hughes, D. W. 2011, *PEPI*, **187**, 78  
 Howes, G. G., & Quataert, E. 2010, *ApJL*, **709**, L49  
 Kraichnan, R. H. 1967, *PhFl*, **10**, 1417  
 Kraichnan, R. H. 1973, *JFM*, **59**, 745  
 Krause, F., & Rädler, K. 1980, *Mean-Field Magnetohydrodynamics and Dynamo Theory* (Berlin: Akademie-Verlag)  
 Lessinnes, T., Plunian, F., & Carati, D. 2009, *ThCFD*, **23**, 439  
 Lessinnes, T., Plunian, F., Stepanov, R., & Carati, D. 2011, *PhFl*, **23**, 035108  
 Linkmann, M., Berera, A., McKay, M., & Jäger, J. 2016, *JFM*, **791**, 61  
 Linkmann, M., & Dallas, V. 2016, *PhRvE*, **94**, 053209  
 Linkmann, M., & Dallas, V. 2017, *PhRvF*, **2**, 054605  
 Linkmann, M., Sahoo, G., McKay, M., Berera, A., & Biferale, L. 2017, *ApJ*, **836**, 26  
 Malapaka, S. K., & Müller, W.-C. 2013a, *ApJ*, **774**, 84  
 Malapaka, S. K., & Müller, W.-C. 2013b, *ApJ*, **778**, 21  
 Mininni, P., Alexakis, A., & Pouquet, A. 2006, *PhRvE*, **74**, 016303  
 Mininni, P. D. 2011, *AnRFM*, **43**, 377  
 Mininni, P. D., Alexakis, A., & Pouquet, A. 2008, *PhRvE*, **77**, 036306  
 Mininni, P. D., Alexakis, A., & Pouquet, A. 2009, *PhFl*, **21**, 015108  
 Mininni, P. D., & Pouquet, A. 2013, *PhRvE*, **87**, 033002  
 Moffatt, H. 1989, *Natur*, **341**, 285  
 Moffatt, H. 2014, *JFM*, **741**, R3  
 Moffatt, H. K. 1969, *JFM*, **35**, 117  
 Moffatt, H. K. 1978, *Magnetic Field Generation in Electrically Conducting Fluids* (Cambridge: Cambridge Univ. Press)  
 Monthus, C. 2018, arXiv:1810.05082  
 Müller, W.-C., Malapaka, S. K., & Busse, A. 2012, *PhRvE*, **85**, 015302  
 Parker, E. N. 1979, *Cosmical magnetic fields: Their origin and their activity* (Oxford: Clarendon Press)  
 Plunian, F., Stepanov, R., & Frick, P. 2013, *PhR*, **523**, 1  
 Pouquet, A., Frisch, U., & Léorat, J. 1976, *JFM*, **77**, 321  
 Rathmann, N. M., & Ditlevsen, P. D. 2016, *PhRvE*, **94**, 033115  
 Rathmann, N. M., & Ditlevsen, P. D. 2017, *PhRvF*, **2**, 054607  
 Sahoo, G., Alexakis, A., & Biferale, L. 2017a, *PhRvL*, **118**, 164501  
 Sahoo, G., & Biferale, L. 2015, *EPJE*, **38**, 114  
 Sahoo, G., Bonaccorso, F., & Biferale, L. 2015, *PhRvE*, **92**, 051002  
 Sahoo, G., De Pietro, M., & Biferale, L. 2017b, *PhRvF*, **2**, 024601  
 Shukurov, A. 2004, arXiv:astro-ph/0411739  
 Steenbeck, M., Krause, F., & Rädler, K.-H. 1966, *ZNatA*, **21**, 369  
 Stepanov, R., Frick, P., & Mizeva, I. 2015, *ApJL*, **798**, L35  
 Sulem, P., She, Z. S., Scholl, H., & Frisch, U. 1989, *JFM*, **205**, 341  
 Tobias, S., Cattaneo, F., Boldyrev, S., et al. 2013, *Ten Chapters in Turbulence* (Cambridge: Cambridge Univ. Press)  
 Vainshtein, S., & Zel'Dovich, Y. B. 1972, *SvPhU*, **15**, 159  
 Verma, M. K., Ayyer, A., & Chandra, A. V. 2005, *PhPI*, **12**, 082307  
 Verma, M. K., & Kumar, R. 2016, *JTurb*, **17**, 1112  
 Waleffe, F. 1992, *PhFl*, **4**, 350  
 Widrow, L. M. 2002, *RvMP*, **74**, 775